Pure Appl. Opt. 4 (1995) 587–598. Printed in the UK

Laser-induced fluorescence spectroscopy of the jet-cooled methylthio radical

Prabhakar Misra†, Xinming Zhu and Hosie L Bryant Jr

Laser Spectroscopy Laboratory, Department of Physics and Astronomy, Howard University, Washington, DC 20059, USA

Received 28 July 1994, in final form 7 February 1995

Abstract. Laser-induced fluorescence excitation and wavelength-resolved emission spectra have been recorded for the methylthio (CH_3S) radical in a supersonic jet environment. Twenty one vibronic bands have been obtained in excitation in the 360–387 nm region with about 0.2 cm^{-1} resolution and assigned to the $\tilde{A}\,^2A_1$–$\tilde{X}\,^2E_{3/2}$ and $\tilde{A}\,^2A_1$–$\tilde{X}\,^2E_{1/2}$ electronic transitions. Fluorescence from five vibronic bands (0_0^0, 3_0^1, 3_0^2, 3_1^2 and $2_0^1 3_1^0$) has been individually dispersed by a 0.6 m monochromator with a resolution of 0.3 nm. To the best of our knowledge, the wavelength-resolved emission spectra of CH_3S for the 3_1^2 and $2_0^1 3_1^0$ bands are being reported here for the first time and these provide new vibrational intervals hitherto unobserved. Fundamental vibrational frequencies have been determined for the ν_2 (umbrella) and ν_3 (C–S stretch) modes of CH_3S for both the excited $\tilde{A}\,^2A_1$ state and the ground $\tilde{X}\,^2E$ state: $\nu_2' = 1096$ cm^{-1}, $\nu_3' = 402$ cm^{-1}, $\nu_2'' = 1328$ cm^{-1} and $\nu_3'' = 742$ cm^{-1}. In addition, the ν_6 (rocking) mode vibrational frequency has been obtained for the $\tilde{A}\,^2A_1$ state, i.e. $\nu_6' = 628$ cm^{-1}. Vibrational and anharmonic parameters have been determined by a least-squares fit of the progressions involving the symmetric ν_3 vibration in the $\tilde{A}\,^2A_1$–$\tilde{X}\,^2E_{3/2}$ excitation spectra and involving both the ν_2 and ν_3 progressions in the dispersed fluorescence spectra.

1. Introduction

The methylthio (CH_3S) molecule is an important free radical intermediate in atmospheric reaction processes and combustion phenomena [1]. It is also known to cause acid precipitation [2]. CH_3S has a ^2E ground electronic state and is subject to Jahn–Teller distortion. It exhibits moderately large (~ 260 cm^{-1}) spin–orbit splitting and provides a good opportunity to examine the interaction between spin–orbit splitting and Jahn–Teller distortion [3, 4].

CH_3S has been studied employing emission [5], laser photodetachment [6, 7], electron paramagnetic resonance [8], matrix IR [9], microwave [10], and laser induced-fluorescence (LIF) techniques [11–13]. However, the spectroscopic information about CH_3S remains incomplete. For example, the fundamental frequencies for the ν_1 ($\mathbf{a}_1$ C–H stretch), ν_4 (e C–H stretch) and ν_5 (e scissors) vibrational modes for both the excited $\tilde{A}\,^2A_1$ and ground $\tilde{X}\,^2E$ states are either unknown or poorly determined. There are no reports in the literature of CH_3S spectra involving the degenerate vibrational (ν_4, ν_5, ν_6) exhibiting Jahn–Teller activity.

In this paper, we report extensive LIF excitation and wavelength-resolved emission spectra of CH_3S obtained with our supersonic jet expansion system. The cooling effect

† Author to whom correspondence should be addressed.

0963-9659/95/050587+12 $19.50

due to the supersonic jet has been observed by changing the time delay between the photolysis beam and the probe beam. Twenty one vibronic bands have been identified in the laser excitation spectra recorded with 0.2 cm^{-1} resolution in the wavelength region 360–387 nm. Wavelength-resolved emission spectra recorded with a resolution of 0.3 nm are being reported here with detailed vibrational assignments for five pumped bands, namely 0_0^0, 3_0^1, 3_0^2, 3_1^2 and $2_0^1 3_1^0$. To the best of our knowledge, dispersed spectra for the 3_1^2 and $2_0^1 3_1^0$ bands are being published here for the *first* time. Vibrational frequencies for the ν_2 (a_1 umbrella) and ν_3 (a_1 C–S stretch) modes of CH_3S have been determined to within an uncertainty of about 15 cm^{-1} for both the excited ($\tilde{A}\,^2A_1$) and ground ($\tilde{X}\,^2E$) states on the basis of our recorded spectra. Vibrational and anharmonic constants have been obtained by a least-squares fit of the progressions involving the ν_3 mode in the $\tilde{A}\,^2A_1$–$\tilde{X}\,^2E_{3/2}$ excitation spectra and involving both the ν_2 and ν_3 modes in the wavelength-resolved emission spectra.

2. Experimental

Methyl disulphide [$(CH_3)_2S_2$]—which is available commercially (Aldrich Chemical Co.)—was selected as the precursor for the CH_3S radical. Helium (at a typical pressure of 200 psi) was the carrier gas and passed through a sample cylinder that contained the precursor at room temperature. The mixture of helium and precursor was introduced into a vacuum chamber through a commercial pulsed valve (General Valve IOTA ONE) of 0.5 mm orifice. The pressure in the evacuated chamber was typically 5×10^{-4} Torr when the pulsed valve was run at 10 Hz with an open duration of 300 μs. Methyl disulphide seeded in the supersonic jet expansion was photolysed by the KrF line (at 248 nm) of an excimer laser (Questek 2000).

The excimer laser beam was focused into the expansion chamber by a quartz lens of focal length 1 metre and directed as close to the nozzle as possible. CH_3S generated *in situ* in the supersonic expansion was then excited by a dye laser (Spectra Physics PDL-3) pumped by a second excimer laser (Questek 2030) operating on the XeCl line (at 308 nm). Exciton dyes BPBD, Exalite 376 and BBQ, were used to generate the requisite range of dye laser wavelengths for recording the laser excitation spectra. The typical dye laser pulse energy was 1–3 mJ and the nominal linewidth of the probe pulse was about 0.07 cm^{-1}. A delay (typically 6 μs) was maintained between the photolysis and probe laser pulses. LIF from the excited CH_3S molecules was collected by a quartz lens ar right angles to the plane containing the counterpropagating laser beams and the supersonic nozzle and was detected by a photomultiplier tube (EMI 9658R). Fluorescence excitation spectra for CH_3S were recorded by scanning the dye laser wavelength. The signals were accumulated and averaged by a boxcar integrator (Stanford Research Systems 250) with a gate-width of 0.5 μs. Wavelength calibration was carried out by an optogalvanic discharge tube [14]. An uncoated quartz wedge was inserted in the optical path of the dye laser beam to pick off two weak beams (each about 5% of the primary pulse energy). One beam enters unfocused through a 2 mm diameter aperture the cathode of an optogalvanic (OG) discharge tube—either a commercial iron–neon hollow cathode lamp (Perkin–Elmer 303) or a galvatron (Hamamatsu L2783-26ANE-FE). When the frequency of the laser pulse equalled the transition frequency for atomic Ne or Ar, the voltage across the OG lamp changed and was recorded through a 0.05 μF capacitor by a second boxcar integrator (Stanford Research 250). The second beam coming off the wedge goes through a diverging lens and illuminates an uncoated,

parallel-faced quartz disc (6 mm thick) at a small angle of about 1–2°. The interference pattern generated by the two reflected beams from the front and rear surfaces of the disc was read by a photodiode through a pinhole. A computer-aided (IBM AT compatible) data acquisition system was used to record the LIF excitation spectrum, the optogalvanic spectrum and the interference pattern simultaneously. Such an approach provided precisely calibrated LIF excitation spectra of the CH_3S radical and yielded vibrational intervals primarily in the excited $\tilde{A}\,^2A_1$ state. When the two lasers were farther apart within the supersonic expansion, the LIF excitation spectra obtained were vibrationally and rotationally colder. To obtain information concerning the vibrational intervals in the ground $\tilde{X}\,^2E$ state, the dye laser was tuned to the wavelength where the radical emitted the strongest fluorescence (within a certain chosen vibronic band). Single vibronic level dispersed fluorescence spectra were then recorded by focusing the total fluorescence onto the entrance slit of a scanning 0.6 metre monochromator (Jobin Yvon HRS 2). Output signal at the exit slit of the monochromator was collected by a photomultiplier tube (Hamamatsu R905) and was relayed to the computer-aided data acquisition system. The gate-width of the boxcar integrator was typically 3 μs. The resolution of the monochromator was estimated to be 0.3 nm for a slit-width of 0.2 mm. Each data point was an average over 10 events and the scan speed for the grating was set at 24 Å per minute. The grating of the monochromator was calibrated with an iron–neon lamp.

3. Results and discussion

By generating the photolysed fragments *in situ* in a supersonic jet expansion, it is possible to study the CH_3S radical under 'cold' conditions. Extensive cooling of the translational and rotational degrees of freedom causes the spectra of the polyatomic CH_3S molecule to be simpler and amenable to detailed spectroscopic analysis. When the delay between the photolysis and probe beams was reduced, the spectra were characteristic of warmer translational temperatures and contained a significantly larger number of transitions. A pair of laser excitation scans are presented in figure 1. Both scans were taken in the region 25 870–26 500 cm^{-1} with the same backing pressure of 200 psi helium, but with two different time delays between the photolysis and probe beams. In figure 1, the top scan was taken with a delay of 3 μs between the photolysis and probe pulses, while the bottom trace was obtained with 8 μs delay. A longer delay between the photodissociation and excitation laser pulses results in a greater number of collisions of the CH_3S radicals with the helium particles comprising the carrier gas and thereby lower translational, vibrational and rotational temperatures in the jet expansion (as seen in the lower trace of figure 1). Occasionally, warmer scans were needed in order to record the weaker vibronic features (escpecially 'hot bands' with $v'' \neq 0$) belonging to the $\tilde{A}\,^2A_1$–$\tilde{X}\,^2E$ electronic system; for example, the 6_1^0, $2_0^1 5_1^0$, 3_1^2 and $6_0^1 3_1^0$ bands clearly seen in the top trace recorded with 3 μs delay, are either barely visible or totally absent in the lower trace of figure 1 taken with a delay of 8 μs. Clearly, the supersonic jet expansion preferentially populates the $v'' = 0$ level as compared with the $v'' = 1$ level in a 'colder' LIF excitation spectrum.

The excitation spectrum of jet-cooled CH_3S in the region 25 800–27 800 cm^{-1} is shown in figure 2 and exhibits four main progressions belonging to the $\tilde{A}\,^2A_1$–$\tilde{X}\,^2E_{3/2}$ electronic system. Two of these progressions are with anharmonically decreasing vibrational spacing (402 to 386 cm^{-1}) and are indicated by 3_1^v and 3_0^v, respectively;

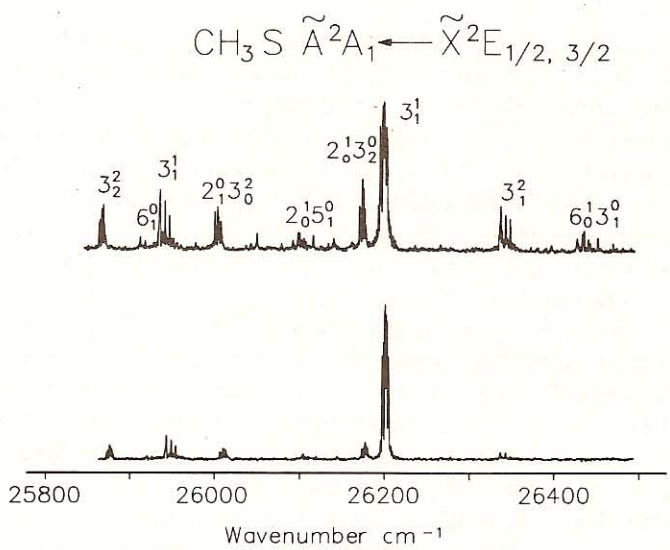

Figure 1. Laser excitation spectrum of $\tilde{A}$–$\tilde{X}$ CH_3S in the region 25 800–26 500 cm^{-1}. The vibrational assignments are indicated in the upper trace. The helium backing pressure was 200 psi and the scan rate 0.2 nm min^{-1}. The delay between the photolysis and probe lasers was 3 μs for the upper trace and 8 μs for the lower trace.

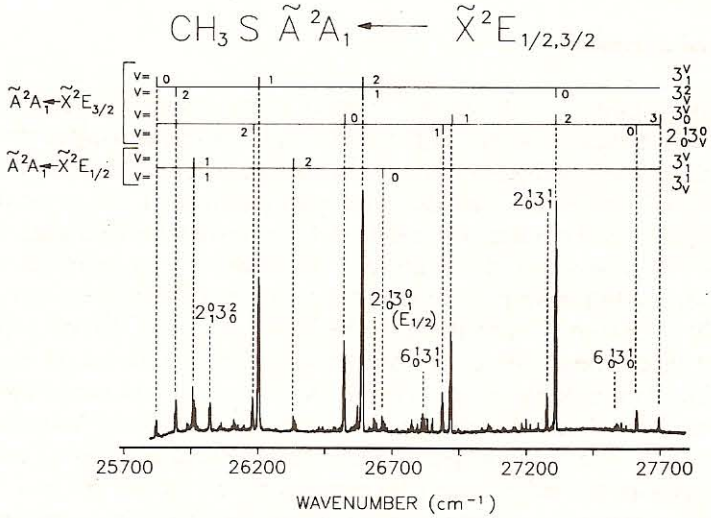

Figure 2. Laser excitation spectrum of CH_3S showing the $\tilde{A}\,^2A_1$–$\tilde{X}\,^2E_{3/2}$ and $\tilde{A}\,^2A_1$–$\tilde{X}\,^2E_{1/2}$ transitions. A backing pressure of 200 psi helium was used, while the delay between the photolysis and probe lasers was 6 μs and the scan rate 0.2 nm min^{-1}. The intensity of the fluorescence was not normalized to the output energy of the excitation laser.

while the remaining two progressions occur with a vibrational interval anharmonicity in the range 734–726 cm^{-1}, and are indicated by 3_v^2 and $2_0^1 3_v^0$ and displayed in figure 2. All of the line positions defining the locations of the different vibronic bands are reported in table 1 and correspond to band maxima.

Bands displaying identical rotational contours were construed to belong to the same electronic transition; and thereby one could separate bands belonging to the $\tilde{A}\,^2A_1$–

Table 1. Observed bands in the CH_3S $\tilde{A}\,^2A_1$–$\tilde{X}\,^2E$ excitation spectra.

$\tilde{A}\,^2A_1$–$\tilde{X}\,^2E_{3/2}$		$\tilde{A}\,^2A_1$–$\tilde{X}\,^2E_{1/2}$		
Wavenumber (cm^{-1})	Relative to 0_0^0 (cm^{-1})	Wavenumber (cm^{-1})	Relative to 0_0^0 (cm^{-1})	Vibrational assignment
25 863	−666			3_2^2
25 908	−621			6_1^0
25 999	−530			$2_1^0 3_0^2$
26 094	−435			$2_0^1 5_1^0$(?)
26 168	−361			$2_0^1 3_2^0$
26 196	−333	25 937	−592	3_1^1
26 430	−99			$3_1^0 6_0^1$
26 529	0			0_0^0
26 597	68	26 339	−190	3_1^2
26 824	295	26 579	50	$3_1^1 6_0^1$
26 898	369	26 640	111	$2_0^1 3_1^0$
26 931	402	26 672	143	3_0^1
27 289	760			$2_0^1 3_1^1$
27 323	794			3_0^2
27 625	1096			2_0^1
27 709	1180			3_0^3

$\tilde{X}\,^2E_{3/2}$ and $\tilde{A}\,^2A_1$–$\tilde{X}\,^2E_{1/2}$ systems, respectively. The $E_{1/2}$ bands exhibited a distinctly different rotational contour as compared to the $E_{3/2}$ bands as illustrated by the 3_0^1 band shown in figure 3. The difference in the rotational structure of the $3_0^1(E_{1/2})$ and $3_0^1(E_{3/2})$ bands is obvious. As clearly seen in figure 3, there are three main peaks (separated by about 6 cm^{-1}) that are accompanied by about twenty small peaks in the $3_0^1(E_{12})$

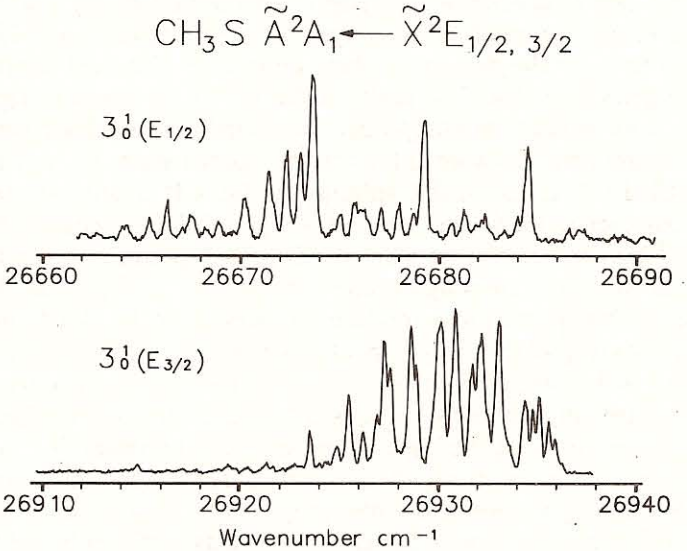

Figure 3. Laser excitation spectrum of the $\tilde{A}$–$\tilde{X}$ 3_0^1 band of CH_3S. The top trace is for $\tilde{X}\,^2E_{1/2}$ and the bottom trace for $\tilde{X}\,^2E_{3/2}$. The helium backing pressure was 200 psi, while the delay between the photolysis and probe lasers was 5 μs and the scan rate 0.05 nm min^{-1}.

spectrum; the majority of these weak features are located on the lower wavenumber side of the strong peaks (see upper trace of figure 3). On the other hand, the $3_0^1(E_{3/2})$ band has its main peaks clustered together at the centre of the band with an $\sim 8\ cm^{-1}$ bandwidth (see lower trace of figure 3).

A separation into $\tilde{A}\,^2A_1$–$\tilde{X}\,^2E_{3/2}$ and $\tilde{A}\,^2A_1$–$\tilde{X}\,^2E_{1/2}$ transitions was consistently made possible owing to the observation of two weak progressions (as shown in figure 2) with vibrational intervals similar to 3_1^v and 3_v^1 (of $\tilde{A}\,^2A_1$–$\tilde{X}\,^2E_{3/2}$), but red-shifted by about $259\ cm^{-1}$ towards the smaller wavenumber excitation region relative to the corresponding lines of the $E_{3/2}$ progression, and were designated as belonging to the $\tilde{A}\,^2A_1$–$\tilde{X}\,^2E_{1/2}$ electronic system. Several new bands (hitherto unreported) have been observed in the present LIF study; while some are shown in figure 2, all of the bands observed have been summarized in table 1. Twenty one vibrational bands can be identified and assigned in the excitation spectrum. The wavenumbers defining the band maximum—along with vibrational assignments—are listed in table 1. The 0_0^0 band was observed at $26\,529\ cm^{-1}$. Fundamental vibrational frequencies of the umbrella ($\mathbf{a}_1\,\nu_2$), the C–S stretch ($\mathbf{a}_1\,\nu_3$) and the rocking ($\mathbf{e}\,\nu_6$) modes determined for the $\tilde{A}\,^2A_1$ state were $\nu_2' = 1096\ cm^{-1}$, $\nu_3' = 402\ cm^{-1}$ and $\nu_6' = 628\ cm^{-1}$, respectively; while those for the $\tilde{X}\,^2E$ state were $\nu_2'' = 1328\ cm^{-1}$ and $\nu_3'' = 742\ cm^{-1}$, respectively. The vibrational assignments were carried out using the similar symmetric top methoxy (CH_3O) molecule as a guide [15]. An additional band seen in the LIF excitation spectra around $26\,094\ cm^{-1}$ was assigned $2_0^1 5_1^0(E_{3/2})$ and thereby yielded $\nu_5'' = 1531\ cm^{-1}$ for the scissor vibrational mode—albeit with some uncertainty, because this $\mathbf{e}\,\nu_5$ mode showed up only once in the excitation scans recorded. The vibrational wavenumbers listed in table 1 are accurate to within an experimental uncertainty of $15\ cm^{-1}$, since the rotational contour observed—especially for the $E_{1/2}$ bands (for example, see the 3_0^1 band displayed in figure 3)—does not allow a more precise determination of the band centre without a meaningful rotational analysis.

Single vibronic level dispersed fluorescence spectra for five bands, namely 0_0^0, 3_1^2, 3_0^1, 3_0^2 and $2_0^1 3_1^0$, are being reported in this paper. To the best of our knowledge, of the above cited wavelength-resolved emission spectra, those for the 3_1^2 and $2_0^1 3_1^0$ bands are being presented here for the *first* time. Three illustrative dispersed fluorescence scans are shown in figures 4–6. The first peak on the left of the scans in figures 4 and 5 corresponds to a mixture of the pump laser wavelength and the fluorescence from the CH_3S transition from the vibrational level in the excited states ($\tilde{A}\,^2A_1$) to that in the ground state ($\tilde{X}\,^2E$). The spin–orbit splitting of the CH_3S ground state is not so obvious—as compared to the $64\ cm^{-1}$ doublet [15] for CH_3O—because of the relatively large splitting of $266\ cm^{-1}$. However, when the dispersed spectra were carefully assigned, it was found that two separate progressions (labelled $^2A_1 \rightarrow {}^2E_{3/2}$ and $^2A_1 \rightarrow {}^2E_{1/2}$ in figures 4–6) involving the various vibrational modes could be clearly identified. The combination modes (e.g. $2_1^0 3_v^1$ and $2_2^0 3_v^1$ involving ν_2 and ν_3) in the wavelength-resolved emission spectra had a smaller frequency than the sum of the individual frequencies owing to the anharmonicity of the vibrations; a difference that increased gradually from 23 to $72\ cm^{-1}$ when involving the higher frequency vibrational modes. Figure 4 shows the dispersed fluorescence spectrum obtained when the 3_0^1 band (at $26\,931\ cm^{-1}$) was pumped and it exhibits prominent doublet progressions with some weak single lines. The separation ($266\ cm^{-1}$) of the doublets corresponds to the spin–orbit splitting in the $\tilde{X}\,^2E$ state. All of the progressions assigned in the 3_0^1 spectrum had consistent vibrational intervals that decreased anharmonically from 738 to $678\ cm^{-1}$ towards the red. These progressions were readily assigned to the ν_3 ($\mathbf{a}_1$ C–S stretching) mode in the

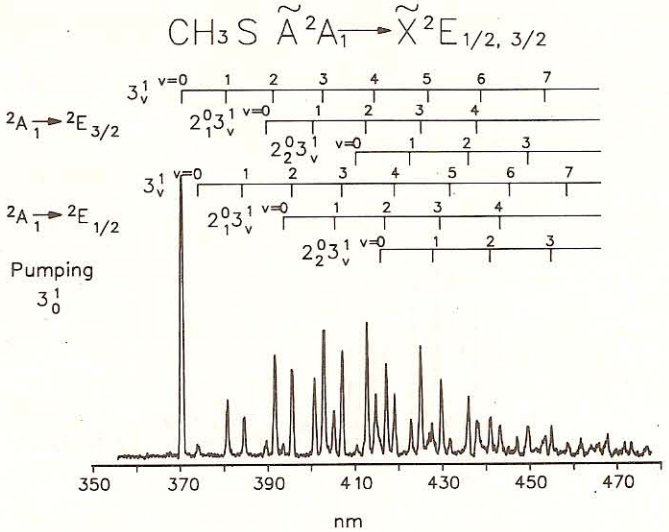

Figure 4. Laser-excited dispersed fluorescence spectrum of jet-cooled CH_3S excited at 26 931 cm^{-1} (3_0^1 band). The resolution of the monochromator was 0.3 nm, while the gate-width of the boxcar integrator was 3 μs, and the scan speed for the grating was set at 24 Å per minute.

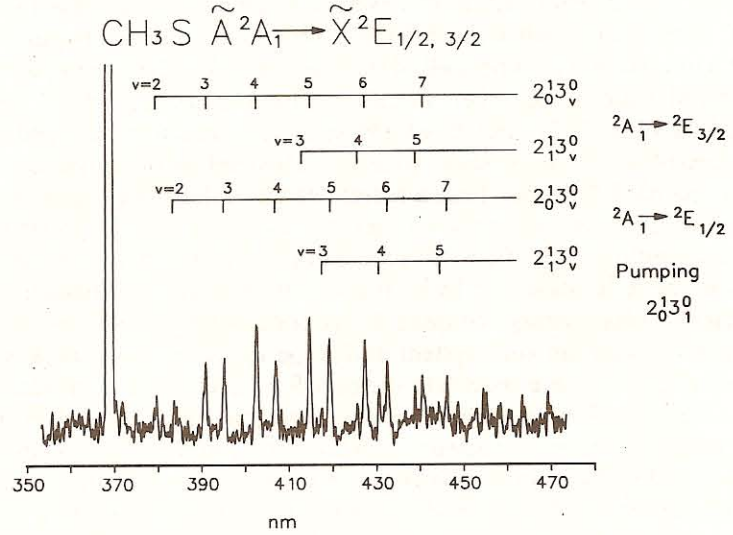

Figure 5. Dispersed fluorescence spectrum of jet-cooled CH_3S excited at 26 898 cm^{-1} ($2_0^1 3_1^0$ band). Other experimental conditions were the same as in figure 4.

$\tilde{X}\,^2E$ state, which is expected to be the most active vibrational mode—akin to the a_1 C–O stretch in the CH_3O radical [15]. There were two other progressions with vibrational spacings starting at 1332 cm^{-1} and 2629 cm^{-1} from the pumped origin, which were assigned to $2_1^0 3_v^1$ and $2_2^0 3_v^1$, respectively, with v representing the vibrational quantum number in the ground state $\tilde{X}\,^2E_{3/2}$. Similarly, the 0_0^0, 3_0^2, 3_1^2 and $2_0^1 3_1^0$ bands were also excited and dispersed. The dispersed fluorescence spectra of CH_3S excited at

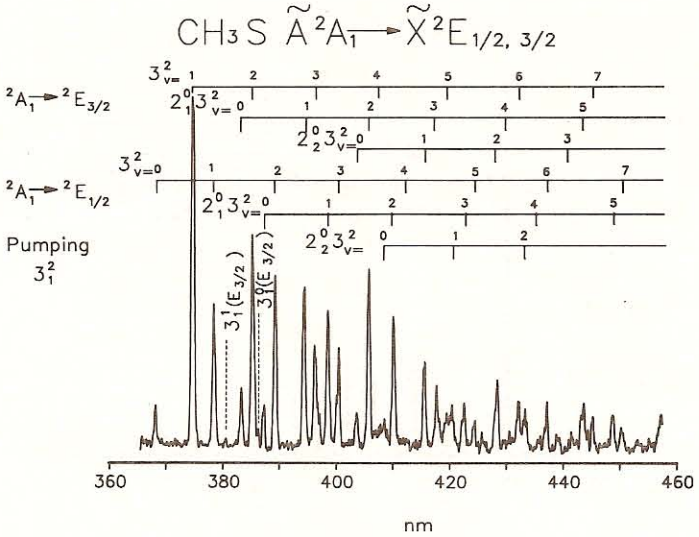

Figure 6. Laser-excited dispersed fluorescence spectrum of jet-cooled CH_3S excited at 26 597 cm^{-1} (3_1^2 band). Other experimental conditions were the same as in figure 4.

26 898 cm^{-1} ($2_0^1 3_1^0$ band) and at 26 597 cm^{-1} (3_1^2 band) are shown in figures 5 and 6, respectively. The intensity variations observed in figures 4–6 are due to changes in the Franck–Condon factors when the different bands were individually pumped. In the five dispersed bands recorded, almost all of the transitions involved the ν_2 and ν_3 vibrations in the ground state. Four other vibrational frequencies, namely ν_1'', ν_4'', ν_5'' and ν_6'', corresponding to $\mathbf{a}_1$ C–H stretch, **e** C–H stretch, **e** scissor mode, and the **e** rocking mode, respectively, in the ^2E state, were not observed in the dispersed spectra of the five bands recorded. One may have a better chance of detecting the above-cited ground state vibrational frequencies in the wavelength-resolved emission spectra by exciting the CH_3S radical within a specific rovibronic band maximum involving the ν_1, ν_4, ν_5 and ν_6 modes in the $\tilde{X}\,^2E$ state and by employing an optical multichannel analyser (OMA) system that includes a charge-coupled device (CCD) detector. We are in the process of putting together such an OMA system and hope to record even weak single vibronic level dispersed fluorescence spectra in the near future. The $\tilde{X}\,^2E\,\nu_3$ mode, corresponding to the $\mathbf{a}_1$ C–S symmetric stretch, gives the strongest emission, and exhibits 'doubled progressions' that show consistent doubling of vibronic features in the dispersed spectrum—the doubling simply referring to the spin–orbit splitting of the ground state. The vibrational intervals observed by pumping bands 0_0^0, 3_0^1 and 3_0^2 in dispersed fluorescence are listed in table 2. Average intervals were determined for the three dispersed bands and consistent vibrational assignments made corresponding to the mean wavenumber interval. These vibrational assignments have been carefully separated into $\tilde{A}\,^2A_1$–$\tilde{X}\,^2E_{3/2}$ and $\tilde{A}\,^2A_1$–$\tilde{X}\,^2E_{1/2}$ transitions. Although the dispersed fluorescence spectrum of band 3_1^2 has a structure similar to that of 3_0^1, it exhibits more transitions and thereby new energy levels. Five such transitions in emission are separated from the pumping frequency by intervals $+599\ cm^{-1}$, $+1910\ cm^{-1}$ $-473\ cm^{-1}$, $+871\ cm^{-1}$ and $+2166\ cm^{-1}$, respectively. These have been respectively assigned $2_1^0 3_0^2$ and $2_2^0 3_0^2$ for $E_{3/2}$, and 3_0^2, $2_1^0 3_0^2$ and $2_2^0 3_0^2$ for $E_{1/2}$. There are two other frequencies, namely 408 cm^{-1} and 804 cm^{-1}, that have been assigned 3_1^1 and 3_1^0 for $E_{3/2}$, respectively, which clearly

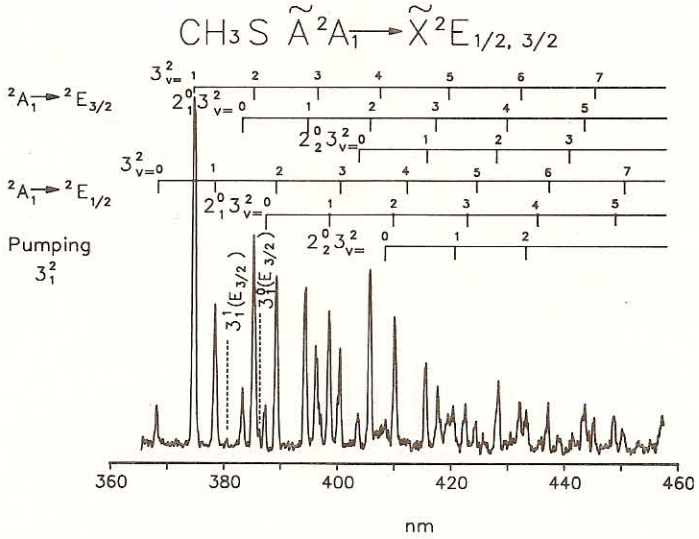

Figure 6. Laser-excited dispersed fluorescence spectrum of jet-cooled CH_3S excited at 26 597 cm^{-1} (3_1^2 band). Other experimental conditions were the same as in figure 4.

26 898 cm^{-1} ($2_0^1 3_1^0$ band) and at 26 597 cm^{-1} (3_1^2 band) are shown in figures 5 and 6, respectively. The intensity variations observed in figures 4–6 are due to changes in the Franck–Condon factors when the different bands were individually pumped. In the five dispersed bands recorded, almost all of the transitions involved the ν_2 and ν_3 vibrations in the ground state. Four other vibrational frequencies, namely ν_1'', ν_4'', ν_5'' and ν_6'', corresponding to $\mathbf{a}_1$ C–H stretch, **e** C–H stretch, **e** scissor mode, and the **e** rocking mode, respectively, in the ^2E state, were not observed in the dispersed spectra of the five bands recorded. One may have a better chance of detecting the above-cited ground state vibrational frequencies in the wavelength-resolved emission spectra by exciting the CH_3S radical within a specific rovibronic band maximum involving the ν_1, ν_4, ν_5 and ν_6 modes in the $\tilde{X}\,^2E$ state and by employing an optical multichannel analyser (OMA) system that includes a charge-coupled device (CCD) detector. We are in the process of putting together such an OMA system and hope to record even weak single vibronic level dispersed fluorescence spectra in the near future. The $\tilde{X}\,^2E\,\nu_3$ mode, corresponding to the $\mathbf{a}_1$ C–S symmetric stretch, gives the strongest emission, and exhibits 'doubled progressions' that show consistent doubling of vibronic features in the dispersed spectrum—the doubling simply referring to the spin–orbit splitting of the ground state. The vibrational intervals observed by pumping bands 0_0^0, 3_0^1 and 3_0^2 in dispersed fluorescence are listed in table 2. Average intervals were determined for the three dispersed bands and consistent vibrational assignments made corresponding to the mean wavenumber interval. These vibrational assignments have been carefully separated into $\tilde{A}\,^2A_1$–$\tilde{X}\,^2E_{3/2}$ and $\tilde{A}\,^2A_1$–$\tilde{X}\,^2E_{1/2}$ transitions. Although the dispersed fluorescence spectrum of band 3_1^2 has a structure similar to that of 3_0^1, it exhibits more transitions and thereby new energy levels. Five such transitions in emission are separated from the pumping frequency by intervals $+599\ cm^{-1}$, $+1910\ cm^{-1}$ $-473\ cm^{-1}$, $+871\ cm^{-1}$ and $+2166\ cm^{-1}$, respectively. These have been respectively assigned $2_1^0 3_0^2$ and $2_2^0 3_0^2$ for $E_{3/2}$, and 3_0^2, $2_1^0 3_0^2$ and $2_2^0 3_0^2$ for $E_{1/2}$. There are two other frequencies, namely 408 cm^{-1} and 804 cm^{-1}, that have been assigned 3_1^1 and 3_1^0 for $E_{3/2}$, respectively, which clearly

Table 2. $CH_3S\,\tilde{X}\,^2E$ vibrational transitions observed in dispersed fluorescence. The numbers listed are the differences between the pump frequency and the corresponding emission frequencies (in cm^{-1}).

	$\tilde{A}\,^2A_1$–$\tilde{X}\,^2E_{3/2}$				$\tilde{A}\,^2A_1$–$\tilde{X}\,^2E_{1/2}$				
Pumped band	0_0^0	3_0^1	3_0^2	Average	0_0^0	3_0^1	3_0^2	Average	Assignment
						263	268	266	
	745	738	743	742	998	1001	997	1000	ν_3
	1326	1332	1325	1328		1583	1595	1589	ν_2
	1463	1464	1464	1464	1723	1722	1718	1721	$2\nu_3$
	2048	2045	2057	2050	2319	2319	2310	2316	$\nu_2 + \nu_3$
	2177	2179	2179	2178	2437	2434	2436	2432	$3\nu_3$
		2629		2629					$2\nu_2$
	2767	2768	2767	2767	3028	3022	3024	3025	$\nu_2 + 2\nu_3$
	2888	2883		2886	3137	3136		3136	$4\nu_3$
	3345	3345	3347	3346		3611		3611	$2\nu_2 + \nu_3$
	3477	3474		3476	3737	3732		3735	$\nu_2 + 3\nu_3$
	3584	3589		3586	3839	3835		3837	$5\nu_3$
	4062	4057		4060	4327	4323		4325	$2\nu_2 + 2\nu_3$
	4168	4167		4168	4431	4431		4431	$\nu_2 + 4\nu_3$
	4269			4269	4527			4527	$6\nu_3$
		4633		4633					$3\nu_2 + \nu_3$
	4757	4752		4754	5021	5017	5019		$2\nu_2 + 3\nu_3$
	4856			4856					$\nu_2 + 5\nu_3$
	4946	4948		4947					$7\nu_3$
	5451			5451					$2\nu_2 + 4\nu_3$
	5529			5529					$\nu_2 + 6\nu_3$

show the occurrence of relaxation in the upper state prior to emission. Because these two bands (3_1^2 and $2_0^1 3_1^0$ $\tilde{X}\,E_{3/2}$) were not excited from the $v_3'' = 0$ level, we list the observed frequencies and the assignments in a separate table 3. Based on the assignments of the various dispersed spectra, the following consistent vibrational frequencies have been determined for CH_3S in the ground state: $\nu_2'' = 1328\ cm^{-1}$ and $\nu_3'' = 742\ cm^{-1}$. All of these ground state vibrational frequencies are within an experimental uncertainty of $15\ cm^{-1}$ and compare well with the same vibrational frequencies determined from an analysis of the laser excitation spectra (see table 1).

The total energy of a polyatomic molecule, neglecting the rotational energy term, is given by [16]

$$T = T_e + G(v_1, v_2 \cdots) \tag{1}$$

where T_e and v are the electronic energy term and the vibrational quantum number, respectively. The vibrational contribution G to the total energy is given by [16]:

$$G(v_1, v_2 \cdots) = \sum \omega_i(v_i + d_i/2) + \sum\sum x_{ik}(v_i + d_i/2)(v_k + d_k/2) + \sum\sum g_{ik} l_i l_k + \cdots . \tag{2}$$

In equation (2), v_i and v_k are vibrational quantum numbers; ω_i are the vibrational frequencies for infinitesimal amplitudes; x_{ik} and g_{ik} are the anharmonicity constants; d_i and d_k refer to the degeneracies (1, 2 or 3) of the vibrations i and k, respectively; and

Table 3. $CH_3S\,\tilde{X}\,^2E$ vibrational transitions observed in dispersed fluorescence and their assignments. The pumped bands are 3_1^2 and $2_0^1 3_1^0$ $\tilde{A}\,^2A_1$–$\tilde{X}\,^2E_{3/2}$. The numbers listed here are the differences between the pump frequency and the corresponding emission frequencies (in cm^{-1}).

Pumped band	3_1^2 $\tilde{A}\,^2A_1$–$\tilde{X}\,^2E_{3/2}$			$2_0^1 3_1^0$ $\tilde{A}\,^2A_1$–$\tilde{X}\,^2E_{3/2}$		
	$\tilde{A}\,^2A_1$–$\tilde{X}\,^2E_{3/2}$	$\tilde{A}\,^2A_1$–$\tilde{X}\,^2E_{1/2}$	Assignment	$\tilde{A}\,^2A_1$–$\tilde{X}\,^2E_{3/2}$	$\tilde{A}\,^2A_1$–$\tilde{X}\,^2E_{1/2}$	Assignment
		−473	3_0^2			
	0	262	3_1^2	0		$2_0^1 3_1^0$
	408		3_1^1	734	1001	$2_0^1 3_2^0$
	599	871	$2_1^0 3_0^2$	1446	1711	$2_0^1 3_3^0$
	730	997	3_2^2	2160	2407	$2_0 3_4^0$
	804		3_1^0	2747	3009	$2_1^1 3_3^0$
	1330	1598	$2_1^0 3_1^2$	2850	3103	$2_0^1 3_5^0$
	1452	1715	3_3^2	3422	3707	$2_1^1 3_4^0$
	1910	2166	$2_2^0 3_0^2$	3533	3796	$2_0^1 3_6^0$
	2041	2304	$2_1^0 3_2^2$	4123	4392	$2_1^1 3_5^0$
	2622	2897	$2_2^0 3_1^2$	4217	4478	$2_0^1 3_7^0$
	2743	3021	$2_1^0 3_3^2$			
	2846	3121	3_5^2			
	3342	3607	$2_2^0 3_2^2$			
	3538	3806	3_6^2			
	4139	4401	$2_1^0 3_5^2$			
	4220	4471	3_7^2			

l_i and l_k are angular momentum quantum numbers of the degenerate vibrations, where

$$l_i = v_i, v_i - 2, v_i - 4, \cdots, 1 \text{ or } 0 \tag{3}$$

and similarly for l_k. For non-degenerate vibrations, $l_i = 0$, and $g_{ik} = 0$.

The wavenumbers of the spectral lines corresponding to transitions between two electronic states are given by [16]

$$v = T' - T'' = T'_e - T''_e + G'(v'_1, v'_2 \cdots) - G''(v''_1, v''_2 \cdots) \tag{4}$$

where a single prime refers to the upper electronic state, a double prime denotes the lower electronic state, and the subscripts indicate the vibrational modes involved in the transition. For $v' = v'' = 0$, $v = v_0$ yields the band origin v_0. The v_3 progressions belonging to the $\tilde{A}\,^2A_1$–$\tilde{X}\,^2E_{3/2}$ electronic system seen in the excitation spectrum of CH_3S were simultaneously fitted by the least-squares method to the following equation [16]:

$$v - v_0 = (\tfrac{1}{2}\omega'_3 - \tfrac{1}{2}\omega''_3 - \tfrac{1}{4}x'_3 + \tfrac{1}{4}x''_3) - \omega'_3(v'_3 + \tfrac{1}{2}) + \omega''_3(v''_3 + \tfrac{1}{2}) + x'_3(v'_3 + \tfrac{1}{2})^2 - x''_3(v''_3 + \tfrac{1}{2})^2. \tag{5}$$

where ω_3, x_3 and v_3 are the vibrational constant, the anharmonic constant, and the vibrational quantum number for the v_3 mode, respectively. The single prime and double prime indicate the excited state and ground state, respectively, for the v'–v'' transitions. Following the least-squares fit, we obtain: $\omega'_3 = 409\ cm^{-1}$, $\omega''_3 = 742\ cm^{-1}$, $x'_3 = 3.8\ cm^{-1}$ and $x''_3 = 4.0\ cm^{-1}$. The standard deviation of the fit was $2.8\ cm^{-1}$. For transitions involving both v_2 and v_3 modes (as listed in table 3), the following equation

Table 4. Fundamental vibrational frequencies (in cm^{-1}) for CH_3S in $\tilde{X}\,^2E$ and $\tilde{A}\,^2A_1$ states.

Mode	ν_1	ν_2	ν_3	ν_4	ν_5	ν_6
$\tilde{X}\,CH_3S$		1328	742			
$\tilde{A}\,CH_3S$		1096	402			628

Table 5. Vibrational and anharmonic parameters (in cm^{-1}) associated with the $\tilde{X}\,^2E_{3/2}$ and $\tilde{X}\,^2E_{1/2}$ states of CH_3S.

$\tilde{X}$	ω_2''	ω_3''	x_2''	x_3''	x_{23}''
$^2E_{3/2}$	1340	743	6.8	5	9
$^2E_{1/2}$	1341	742	7.7	4.1	7

was used for the least-squares fit [16]:

$$\nu_0 - \nu = (-\tfrac{1}{2}\omega_2'' - \tfrac{1}{2}\omega_3'' + \tfrac{1}{4}x_2'' + \tfrac{1}{4}x_3'' + \tfrac{1}{4}x_{23}'') + \omega_2''(v_2'' + \tfrac{1}{2}) + \omega_3''(v_3'' + \tfrac{1}{2}) - x_2''(v_2'' + \tfrac{1}{2})^2 - x_3''(v_3'' + \tfrac{1}{2}) - x_{23}''(v_2'' + \tfrac{1}{2})^2(v_3'' + \tfrac{1}{2}). \quad (6)$$

We obtained $\omega_2'' = 1340\ cm^{-1}$, $\omega_3'' = 743\ cm^{-1}$, $x_2'' = 6.8\ cm^{-1}$, $x_3'' = 5\ cm^{-1}$ and $x_{23}'' = 9\ cm^{-1}$ for the $\tilde{X}\,^2E_{3/2}$ state; and $\omega_2'' = 1341\ cm^{-1}$, $\omega_3'' = 742\ cm^{-1}$, $x_2'' = 7.7\ cm^{-1}$, $x_3'' = 4.1\ cm^{-1}$ and $x_{23}'' = 7\ cm^{-1}$ for the $\tilde{X}\,^2E_{1/2}$ state. The standard deviations of the fit were $3\ cm^{-1}$ and $2\ cm^{-1}$ for $\tilde{X}\,^2E_{3/2}$ and $\tilde{X}\,^2E_{1/2}$, respectively. The vibrational frequencies and anharmonic constants determined in the present study are collected together in tables 4 and 5, respectively, and these parameters compare favorably with those cited in earlier reports [12, 13]; any noticeable differences being within our experimental error. We were unable to fit similarly the ν_1, ν_4, ν_5 and ν_6 vibrational modes because there were not adequate members forming progressions involving these vibrations.

In summary, a comprehensive LIF study of the jet-cooled CH_3S radical has enabled recording and identification of 21 vibronic bands in excitation in the 360–387 nm region with $0.2\ cm^{-1}$ resolution. The observed vibrational intervals have been separated into two groups, one corresponding to the $\tilde{A}\,^2A_1$–$\tilde{X}\,^2E_{3/2}$ electronic transition and the other to $\tilde{A}\,^2A_1$–$\tilde{X}\,^2E_{1/2}$. Fluorescence from the $\tilde{A}\,^2A_1$ state was dispersed employing a 0.6 m monochromator with 0.3 nm resolution and wavelength-resolved emission spectra obtained for five pumped bands, namely 0_0^0, 3_0^1, 3_0^2, 3_1^2 and $2_0^1 3_1^0$. Of these vibronic bands, single vibronic level dispersed fluorescence spectra for the 3_1^2 and $2_0^1 3_1^0$ bands have been recorded and analysed for the *first* time. A detailed analysis of the vibrational intervals in the laser excitation and dispersed fluorescence spectra has allowed accurate determination of fundamental vibrational frequencies for the ν_2 (a_1 umbrella) and ν_3 (a_1 C–S stretch) modes of CH_3S for both the $\tilde{A}\,^2A_1$ and $\tilde{X}\,^2E$ states. All of the vibrational assignments are consistent to within a deviation that is estimated to be less than $15\ cm^{-1}$. A least-squares fit of the ν_3 progression seen in the $\tilde{A}\,^2A_1$–$\tilde{X}\,^2E_{3/2}$ excitation spectra and both the ν_2 and ν_3 progressions present in the single vibronic level dispersed

fluorescence spectra allowed determination of significant vibrational and anharmonic parameters for the CH_3S molecule.

Acknowledgments

Financial support from the US Environmental Protection Agency's Office of Exploratory Research (Grant No R819720-01-0), the NASA Lewis Research Center (Grant No NAG3-1677) and the Center for the Study of Terrestrial and Extraterrestrial Atmospheres (Grant No NASA NAGW-2950) is gratefully acknowledged.

References

[1] Foster S C and Miller T A 1989 *J. Phys. Chem.* **93** 5986–99
[2] Mellouki A, Jourdian J L and Le Bras G 1988 *Chem. Phys. Lett.* **148** 231–6 and references therein
[3] Liu X, Damo C P, Lin T-Y D, Foster S C, Misra P, Yu L and Miller T A 1989 *J. Phys. Chem.* **93** 2266–75
[4] Brown J M 1971 *Mol. Phys.* **20** 817–34
[5] Ohbayashi K, Akimoto H and Tanaka I 1977 *Chem. Phys. Lett.* **52** 47–9
[6] Engelking P C, Ellison G B and Lineberger W C 1978 *J. Chem. Phys.* **69** 1826–32
[7] Janousek B K and Brauman J I 1980 *J. Chem. Phys.* **72** 694–700
[8] Gillbro T 1974 *Chem. Phys.* **4** 476–82
[9] Jacox M E 1983 *Can. J. Chem.* **61** 1036–43
[10] Endo Y, Saito S and Hirota E 1986 *J. Chem. Phys.* **85** 1770–7
[11] Hsu Y-C, Liu X and Miller T A 1989 *J. Chem. Phys.* **90** 6852–7
[12] Chiang S-Y and Lee Y-P 1991 *J. Chem. Phys.* **95** 66–72
[13] Suzuki M, Inoue G and Akimoto H 1984 *J. Chem. Phys.* **81** 5405–12
[14] Zhu X, Nur A and Misra P 1994 *J. Quant. Spectrosc. Radiat. Transfer* **52** 167–77
[15] Misra P, Zhu X, Hsueh C-Y and Halpern J B 1993 *Chem. Phys.* **178** 377–85
[16] Herzberg G 1966 *Molecular Spectra and Molecular Structure, III. Electronic Spectra and Electronic Structure of Polyatomic Molecules* (New York: Van Nostrand Reinhold)